Growing exposure and uncertain rainfall trends highlight the critical need for climate resilience in Colombia and Venezuela

Authors

Mariam Zachariah, *Centre for Environmental Policy, Imperial College, London, UK*
Lina Isabel Ceballos-Bonilla, *Sistema de Alerta Temprana de Medellín y el Valle de Aburrá (SIATA), Área Metropolitana del Valle de Aburrá (AMVA), Colombia*
Julián Sepúlveda-Berrío, *Sistema de Alerta Temprana de Medellín y el Valle de Aburrá (SIATA), Área Metropolitana del Valle de Aburrá (AMVA), Colombia*
Paola A. Arias, *Grupo GIGA, Escuela Ambiental, Facultad de Ingeniería, Universidad de Antioquia, Medellín, Colombia*
Joyce Kimutai, *Centre for Environmental Policy, Imperial College, London, UK*
Roop Singh, *Red Cross Red Crescent Climate Centre, The Hague, The Netherlands (based in New Jersey, USA)*
Maja Vahlberg, *Red Cross Red Crescent Climate Centre, The Hague, the Netherlands (based in Ubmeje/Umeå, Sweden)*
Karina Izquerido, *Red Cross Red Crescent Climate Centre, The Hague, The Netherlands (based in Mexico City, Mexico)*
Friederike Otto, *Centre for Environmental Policy, Imperial College, London, UK*

Review authors

Sjoukje Philip, *Royal Netherlands Meteorological Institute (KNMI), De Bilt, The Netherlands*
Izidine Pinto, *Royal Netherlands Meteorological Institute (KNMI), De Bilt, The Netherlands*
Catalina Jamie, *Red Cross Red Crescent Climate Centre, The Hague, The Netherlands (based in Bogotá, Colombia)*
Dora Vrkić, *Grantham Institute - Climate Change and the Environment, Imperial College London, London, UK*

Main findings

- Landslides are common in Colombia and Venezuela during the rainy season due to steep slopes and loose soils. The rapid growth of population and informal settlements in areas prone to landslides, particularly in Colombia, puts people and infrastructure at risk. These informal communities are growing as a result of rapid urbanization as more people move to cities for economic prospects, and in Colombia many of those people are also displaced as a result of violence and conflict.
- Deforestation and the conversion of the Páramos to agricultural land, mining concessions, and overgrazing have reduced the natural ecosystems ability to regulate rainfall-induced floods and increased susceptibility to landslides.
- People who are internally displaced, dealing with economic instability, or affected by conflict, are doubly vulnerable. When combined with recurring climate hazards, this erodes their resilience over time.
- Based on gridded data-products, we find that neither the seasonal (April to June, AMJ) rainfall event over the Colombian Andes nor the Rx5day over the Venezuelan Llanos was particularly extreme from a meteorological point of view with a return period of about 10 and 3 years, respectively.
- When comparing the AMJ event today with the same event in a 1.3°C cooler climate, we find a decrease in the likelihood and intensity of seasonal rainfall as observed by about 12%, but with a large uncertainty around this estimate and 1 out of the 3 data sets showing an increase. Similar results are found for the Rx5day event over the Venezuelan Llanos, where two out of three data sets show a drying trend, leading to an overall 9% decrease in the intensity of heavy precipitation.
- To quantify the role of human-induced climate change in these changes in likelihood and intensity we also analyse climate model data over the study regions for the historical period. The models show some disagreement for the AMJ Colombian Andes event, with some simulating an increase and others indicating decreases in seasonal rainfall. However, a majority show a decreasing trend. The disagreement between individual models is more pronounced for the Rx5day Venezuelan Llanos event, where some show a significant drying, while others show an increase in heavy rainfall.
- These results are aligned with published research. The most recent (2021) IPCC report showed that for Northern South America, the region encapsulating the Orinoco basin, particularly the Venezuelan Llanos, has high uncertainties with respect to observed trends. It projects a drying for seasonal rainfall, especially in June, July and August, but also an increase in the likelihood and intensity of heavy rainfall such as measured as Rx5day with future warming. Moreover, projections of precipitation in North-Western South America, the region containing the Colombian Andes, exhibit large uncertainty, with low confidence in the projections. These changes highlight how climate change affects different weather regimes in different ways, which models can struggle to represent accurately.
- Taken together our results suggest that wet years such as this and the last will continue to occur, while the observed drying, that is more consistent in the east of the analysed regions, implies an increased risk of dry years. The region needs to be prepared for more frequent and more intense droughts and wildfires. However, it also needs to prepare for the possibility of more intense downpours, particularly given uncertainty in the results and research showing

that sub-daily bursts of rainfall can increase even in regions that are experiencing drying trends on longer timescales.
- Collecting, maintaining and sharing high-quality weather data is crucial for understanding changing risks and building resilience against different types of extreme weather. This is especially important for countries with complex rainfall processes, such as Colombia and Venezuela. The relatively wide uncertainties in our analyses highlights the need for long-term in-situ observations and the need for better understanding and representation of the relevant processes in the climate models. It also reflects a broader scientific inequality between the global north and the global south (e.g., WWA DRC floods, 2023) and an ongoing need to invest in weather monitoring stations and climate science to understand changing weather extremes in northern South America.

1 Introduction

In late June 2025, relentless heavy rains battered Colombia and Venezuela for several days, triggering landslides, river overflows, and widespread flooding across the region. One of the most severe incidents occurred in Colombia, where a major landslide struck Granizal, near the city of Medellín, killing 27 people (Alcaldía Bello, 7 July, 2025). Meanwhile, Venezuela experienced several smaller, though still disruptive, landslides around the same time in San Miguel, Niquitao, Mosquey, and across the parishes of Guaramacal and Vega de Guaramacal. These events cut off access to remote areas and heightened risks for rural communities (The Watchers, 25 June, 2025). The states of Mérida, Trujillo, and Táchira were among the worst impacted regions in Venezuela. Sustained rainfall in these parts led to the rivers Motatán and Burate to overflow damaging infrastructure, flooding homes and sweeping away buildings and vehicles (The Watchers, 25 June, 2025). By 26 June, more than 4700 people had been displaced in the affected areas, prompting a national emergency declaration (ReliefWeb, 26 June, 2025).

The rainy season, which typically begins around mid-March, started in early February this year and was significantly wetter than usual. There were multiple heavy rains, with rainfall reaching up to three times the monthly average, for February and April, and were well-forecast by various national meteorological agencies including the Colombian Institute of Hydrology, Meteorology, and Environmental Studies (IDEAM) (The City Paper, 1 April 2025) and Venezuela's National Institute of Meteorology and Hydrology (INAMEH) (IFRC, 20 June 2025). Rainfall in these regions during this time of the year is primarily linked to the migration of the Intertropical Convergence Zone (ITCZ) and tropical waves (more active since June). These are elongated atmospheric disturbances that disrupt wind patterns and pressure systems in the tropics, leading to abundant cloudiness, prolonged heavy rainfall, thunderstorms and strong winds (MeteorologíaenRed, 22 June 2025) in northern South America (Giraldo-Cardenas et al., 2022). Moreover, the complex topography of the region favours the occurrence of orographic lifting which can trigger heavy precipitation events (Poveda et al., 2020; Robledo et al., 2024). Several regions of Latin America, including Colombia and Venezuela, experienced a notable intensification of rainfall and adverse weather events in the last week of June 2025, due to the passage of multiple such tropical waves, the first of which arrived on 24 May. In particular, it was the ninth wave of the season (Tropical Wave 9) interacting with the ITCZ that led to the heavy downpour on the 24th of June (ReliefWeb, 3 July 2025). Based on nearby ground stations of the Early Warning System of Medellín and the Aburrá Valley (SIATA), a risk management strategy from the local environmental agency (AMVA), the cumulative precipitation on the June 23-24 event was around 70 mm, which corresponds to approximately 80% of the climatological value for June in that station. The total precipitation during the month was 2.6 times the monthly average, near normal in May and 2.2 times the monthly April average, making April 2025 the rainiest month in 14 years over the Aburra Valley (SIATA, 2025; ElColombiano, 2025), where the landslide occurred. It is also worth highlighting that in early 2025, a weak La Niña event was present in the Pacific Ocean, and the convective phases of the Madden-Julian Oscillation (MJO) were active during certain weeks, coinciding with increased precipitation. However, during the 24th of June the MJO was in phases 3-4, which are not convective phases over the region.

This year, approximately 230,000 people have been affected across multiple departments and 87 municipalities of Colombia and Venezuela. Flash floods along the Caquetá, Fragua Grande, Congor, Tambor, and Mocoa rivers have caused extensive damage to homes, crops, and livestock. In El Carmen del Darién, Chocó, Colombia, around 20,000 families have been impacted, with the loss of 5,000 hectares of crops compounding the crisis. Health concerns are growing, particularly among children under five, with rising cases of respiratory infections, acute diarrhoeal disease, and vomiting. School closures have further disrupted education and increased community vulnerability.

Diverse impacts have been detected in Colombia. For instance, in Puerto Carreño, Vichada, located on the Orinoco river bank, on the border between Colombia and Venezuela, over 6,000 individuals were affected, with outbreaks of dengue, respiratory issues, and skin conditions reported. Meanwhile, Huila, located in the Colombian Andes, has lost around 100 hectares of coffee crops, adding to the economic toll. In Villavicencio, damage to the aqueduct system has led to water rationing, and water tankers are being used for distribution. In Putumayo, more than 5,800 families have been affected, while in Caquetá, dozens of cattle have been evacuated. In Boyacá, a landslide has displaced at least 90 families and rendered roads impassable, cutting off access for transporting crops and livestock. Approximately 150 hectares were affected by the landslide. In Caldas, 52 families have been impacted by similar events, and it is estimated that at least 2 billion pesos will be required to rehabilitate critical infrastructure in the region (Noticias Caracol, 2025).

In Venezuela, the most severely affected areas are located in the western part of the country, particularly in rural Andean regions, where the overflow of several local rivers and their tributaries has completely disrupted daily life in numerous villages. These flooded regions are responsible for producing 70 per cent of the vegetables consumed nationwide (Moleiro, 2025). Infrastructure has also suffered significant damage, with 25 bridges in the region impacted and 16 of them completely destroyed. Among the most critical losses was the collapse of a major bridge in Portuguesa state, a vital link connecting the Venezuelan Andes with the central part of the country (France 24, 2025).

1.1 Seasonal and extreme rainfall in Colombia and Venezuela

According to the Intergovernmental Panel on Climate Change (IPCC) Sixth Assessment Report (AR6), the regions of North-Western South America (NWS) and Northern South America (NSA)—as defined in the IPCC's regional breakdown (Iturbide et al., 2020)—exhibit differing climate projections, with varying levels of confidence. The Venezuelan Llanos region we look at here is within the NSA region, while the Colombian Andes region is part of the NWS region. For NSA, there is medium confidence in an increase in heavy precipitation events under both 1.5°C of warming and higher scenarios (IPCC WGI Chapter 11). However, average precipitation is projected to decrease during both December–February (DJF) and June–August (JJA), according to the IPCC WGI Atlas chapter. More recent studies show an increased occurrence of dry extremes in the Venezuelan Llanos, located within the NSA IPCC region (Feron et al., 2024). Projections for this region indicate a drying trend in annual precipitation (Arias et al., 2021; Salas et al., 2024). In contrast, NWS shows low confidence in most projected precipitation changes (IPCC WGI Chapter 11), reflecting high uncertainty in the region's response to global warming. The IPCC WGI Atlas suggests a slight increase in precipitation during DJF, but this signal only becomes clear under 3°C of warming or higher. For JJA, projections indicate virtually no change, but as with DJF, the uncertainty is substantial across all scenarios. The large uncertainty of precipitation projections in the Colombian Andes is highlighted by further studies (Arias et al., 2021, 2023).

The IPCC AR6 also reports a significant increase in flood risk for Colombia due to climate change, stating that if global temperatures increase by 1.5°C, the number of people exposed to river flooding in Colombia could rise by 100 to 200% (IPCC, 2022). NWS is well known for being prone to compound mountain hazards like flash floods, debris flows, mountain torrents, and landslides (Guns and Vanacker, 2013; Aristizábal et al., 2020, 2022; Poveda et al., 2020; Arango et al., 2021; Cullen et al., 2022). This is the result of the combination of geomorphology features associated with the steep slopes of the eastern flank of the eastern Andes cordillera in Colombia, hydrometeorological processes that produce large amounts of rainfall, and land use changes over the region (e.g. Guns and Vanacker, 2013; Espinoza et al. 2020; Poveda et al., 2020). An inventory of landslides in Colombia during the 1900-2016 period (a total of 32.022 events) shows that 93% of the recorded landslides occurred in the Colombian Andes, with 92% of these being triggered by rainfall (Aristizábal & Sánchez, 2020).

Rainfall variability in Colombia and Venezuela is shaped by a complex interplay of topographic and atmospheric drivers. The ITCZ dictates the broad seasonal cycle, with its latitudinal migration responsible for the bimodal cycle in the Andes region and unimodal cycle in the Llanos plains and the Caribbean coast (Urrea et al., 2019). Intense storms in the Andes region in Colombia feature strong spatiotemporal variability, which is driven by the steep orography, topographic roughness, local circulations as well as both large- and small-scale convective and wind systems (Poveda et al., 2020). Large-scale teleconnections—primarily, the El Niño–Southern Oscillation (ENSO)—induce strong interannual variability. On average, positive ENSO phases (El Niño) are associated with reduced rainfall and high temperatures across NSA, whereas negative phases (La Niña) typically bring cooler conditions and increased rainfall to the region (Poveda et al., 2006, 2011). Consequently, ENSO events play a significant role in modulating the frequency and severity of hydroclimatic weather extremes such as droughts and floods, depending on the affected region as well as on the ENSO phase and onset characteristics (Sayol et al., 2022). The MJO that acts on 30-60 day time scales also enhance convection moisture flux in this region (Recalde-Coronel et al., 2020), in particular during phases 1, 2, 7 and 8, corresponding to the initial and final stages of the convective phase. On shorter time scales (from days to weeks), tropical waves such as the easterly waves organize convection over the region, triggering precipitation on synoptical spatial scales, which can be further modulated by the MJO (Giraldo-Cardenas et al., 2022).

1.2 Event Definition

In order to fully capture the extent of the impacts associated with the rainfall around June 24—and particularly the landslides along the Andean region in Colombia and Venezuela, and the flooding in the Venezuelan Llanos region—we consider two event definitions:

1. Given the known role of prolonged and intense rainfall leading to soils becoming supersaturated, which heightens the risk of landslides on hill slopes, combined with wetter than normal rainfall in these parts which persisted since April this year, we use the total rainfall during April-May-June (AMJ) for defining the event that led to the landslides in the Andean region in Colombia and Venezuela. For the spatial domain, we use a climatologically homogeneous region covering the Magdalena river catchment over Colombia, which covers most of the Colombian Andes), and the Falcón and Maracaibo basins in Venezuela where the reported landslide sites are located. The wetter than normal seasonal accumulated rainfall during AMJ 2025 over the region is shown in Figure 1(a). The study domain is highlighted in red.

2. Although various parts of Venezuela have been experiencing heavy rainfall since May 2025 on account of the eight tropical waves that passed through the region, our focus is on the heavy rainfall spell on the 24th of June, associated with the flooding in the Venezuelan Llanos. The study region comprises the states of Barinas, Tachira, Trujillo, Mérida, Portuguesa and Apure. The flooding was triggered by the ninth of these tropical waves which arrived around the 20th of June and likely intensified already saturated conditions ([ReliefWeb, 10 July 2025]). For the temporal definition, we focus on the annual maximum 5-day rainfall (annual Rx5day), area-averaged over the study region. Figure 1(b) shows the heaviest 5-day rainfall spell in 2025, during 20-24 June 2025, with the study area highlighted in red.

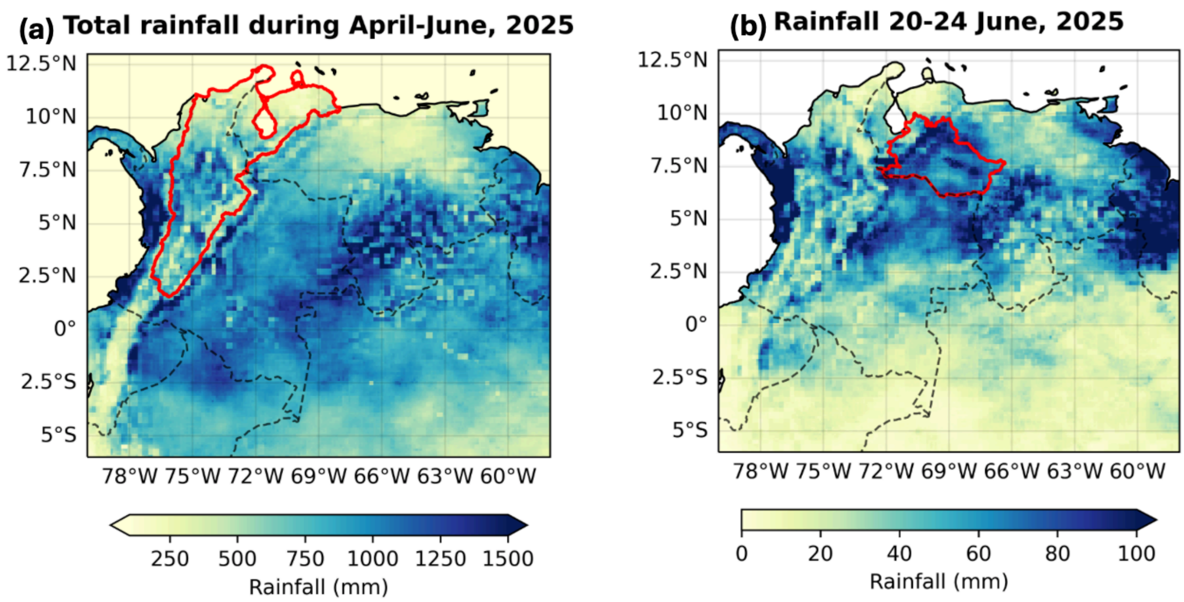

Figure 1.1 *Event definition. a) Total rainfall during AMJ 2025 in Colombia and Venezuela. The red highlighted region corresponds to the Magdalena river basin in Colombia and the Falcón and Maracaibo basins in Venezuela. b) Accumulated rainfall during the period 20-24 June 2025 in*

Colombia and Venezuela. The red contour shows the Venezuelan Llanos affected by heavy rainfall. Source: MSWEP.

In this report, we study the influence of anthropogenic climate change by comparing the likelihood and intensity of similar AMJ rainfall and annual Rx5day events over the respective study regions at present with those in a 1.3°C cooler climate. We also extend this analysis into the future by assessing the influence of a further 1.3°C of global warming from present. This is in line with the latest Emissions Gap Report from the United Nations Environment Programme, which shows that the world is on track for at least 2.6°C temperature rise given currently implemented policies (UNEP, 2024).

2 Data and methods

2.1 Observational data

We first use observational and reanalysis data to estimate the return period of a similar event in the present day and to assess the historical trends with increasing Global Mean Surface Temperature (GMST). The datasets used are as follows:

1. **ERA5**: The European Centre for Medium-Range Weather Forecasts's 5th generation reanalysis product, ERA5, is a gridded dataset that combines historical observations into global estimates using advanced modelling and data assimilation systems (Hersbach et al., 2020). We use daily precipitation data from this product at a resolution of 0.5°×0.5°, from the years 1950 to present. The re-analysis is available until the end of May 2025. We extend the reanalysis data with the ECMWF analysis (1-24 June 2025) and the ECMWF forecast (25-29, June 2025) to cover the period of the event.

2. **Multi-Source Weighted-Ensemble Precipitation (MSWEP):** MSWEP v2.8 dataset (updated from Beck et al., 2019) is fully global, with precipitation available at 3-hourly intervals and at 0.1° spatial resolution, available from 1979 to ~3 hours from real-time. This product combines gauge-, satellite-, and reanalysis-based data.

3. **CHIRPS**: This rainfall product is developed by the University of California (UC) at Santa Barbara Climate Hazards Group, called “Climate Hazards Group InfraRed Precipitation with Station data” (CHIRPS; Funk et al. 2015). Daily data are available at 0.05° resolution, from 1981 to 31 May 2025. The product incorporates satellite imagery with in-situ station data.

Finally, as a measure of anthropogenic climate change, we use the (low-pass filtered) GMST, where GMST is taken from the National Aeronautics and Space Administration (NASA) Goddard Institute for Space Science (GISS) surface temperature analysis (GISTEMP, Hansen et al., 2010 and Lenssen et al. 2019).

2.2 Model and experiment descriptions

We use 2 multi-model ensembles from climate modelling experiments using very different framings (Philip et al., 2020): Sea Surface temperature (SST) driven global circulation high resolution models, coupled global circulation models and regional climate models.

1. **Coordinated Regional Climate Downscaling Experiment CORDEX-CORE (6 models at 0.22° resolution (SAM-22)) multi-model ensemble (Giorgi and Gutowski, 2015; Giorgi et al., 2021).** These simulations are composed of historical simulations from 1970-2005, and projections up to the year 2100 for different Representative Concentration Pathways (RCP, van Vuuren et al., 2011). In this study, the projections under RCP8.5 scenario are used to extend the historical simulations for the models considered. In this study, the first ensemble members from six RCM-GCM pairs that were available for download at the time of the analysis were evaluated for their fidelity in modelling precipitation features in the region.

2. **HighResMIP SST-forced model ensemble (Haarsma et al. 2016), the simulations for which span from 1950 to 2050.** The SST and sea ice forcings for the period 1950-2014 are obtained from the 0.25° x 0.25° Hadley Centre Global Sea Ice and Sea Surface Temperature dataset that have undergone area-weighted regridding to match the climate model resolution. For the 'future' time period (2015-2050), SST/sea-ice data are derived from RCP8.5 (CMIP5) data, and combined with greenhouse gas forcings from SSP5-8.5 (CMIP6) simulations (see Section 3.3 of Haarsma et al. (2016) for further details). Simulations from 11 models under this experiment are considered in this study.

2.3 Statistical methods

Methods for observational and model analysis and for model evaluation and synthesis are used according to the World Weather Attribution Protocol, described in Philip et al., (2020), with supporting details found in van Oldenborgh et al., (2021), Ciavarella et al., (2021), Otto et al., (2024) and here. The key steps, presented in sections 3-6, are: (3) trend estimation from observations; (4) model validation; (5) multi-method multi-model attribution; and (6) synthesis of the attribution statement.

As discussed in Section 1.2, we analyse the time series of AMJ rainfall in the study region defined over the landslide-prone Colombian Andean region, and the annual maximum 5-day rainfall over the region in the Venezuelan Llanos that was severely impacted by the rains and flooding this year.

Nonstationary-normal and nonstationary-Generalized Extreme Value (GEV) distributions that assume GMST as the covariate are used to model AMJ rainfall and annual Rx5day, respectively. The distributions are assumed to scale exponentially with the covariate, with the dispersion (the ratio between the standard deviation and the mean) remaining constant over time. This formulation reflects the Clausius Clapeyron relation, which implies that precipitation scales exponentially with temperature (Trenberth et.al., 2003, O'Gorman and Schneider 2009). The parameters of the statistical model are estimated using maximum likelihood.

For each time series we calculate the return period and intensity of the event under study for the 2025 GMST and for 1.3°C cooler GMST: this allows us to compare the climate of now and of the preindustrial past (1850-1900, based on the Global Warming Index), by calculating the probability ratio (PR; the factor-change in the event's probability) and change in intensity of the event.

3 Observational analysis: return period and trend

3.1 Analysis of gridded data

Figures 3.1 and 3.2 shows the trends and the return period curves (in 2025 climate and a 1.3°C cooler climate as compared to today that is representative of the pre-industrial era before humans began warming the climate), for the seasonal (AMJ) rainfall over the Colombian Andes and the annual Rx5day over the Venezuelan Llanos regions, respectively. The normal distribution is a good fit for the AMJ rainfall time series over the Colombian Andes, across all three datasets. Similarly, the GEV is found to be a good fit for the annual Rx5day series over the Venezuelan Llanos, for all datasets.

The seasonal (AMJ) rainfall over the Colombian Andes region shows a drying tendency under increasing GMST in all three datasets (Figures 3.1(a,b,c)), but less pronounced in CHIRPS (Figure 2(c)). Consequently, the return period curves (Figures 3.1(d-f)) also illustrate this drying tendency further, and likewise show that the seasonal rainfall this year—which is not rare even in today's climate (1-in-11 year events in the ERA5 and MSWEP datasets rounded to 10 years; see Table 3.1 for the exact estimates and the 10-90% confidence intervals)—would have been even more frequent in a 1.3°C cooler world. The CHIRPS dataset did not yet include the event at the time of the analysis and could not be used to calculate the return period of the event. The PR in the ERA5 and MSWEP datasets is 0.18 (see Table 3.2), which implies that the event would have been ~ (1/0.18) or 5.5 times more likely had there been no climate change, and 14-16% wetter. While the trends in CHIRPS qualitatively show the drying tendency in AMJ rainfall due to global warming, the PR and the intensity changes suggest that the event would have been twice as likely without climate change and ~5% wetter.

The annual Rx5day over the Venezuelan Llanos also shows a drying tendency in the ERA5 and MSWEP datasets (Figure 3.2 (a,b)), while CHIRPS shows a strong wetting tendency (Figure 3.2 (c)). From the return period curves, the 2025 event is approximately a 1-in-3-year event in today's climate (Figure 3.2(d-e), Table. 3.1) in the ERA5 and MSWEP datasets. As for the seasonal analysis, the CHIRPS dataset did not yet include the event at the time of the analysis, however the intensity of a 1-in-3 year in today's climate in CHIRPS is comparable to ERA5 (see Table 3.2). The PR estimates suggest that the event is approximately 2-4 times less likely in today's climate (1/0.28=3.57 in MSWEP and 1/0.45=2.22 in ERA5) and 15-22% drier, as compared to the pre-industrial climate. In CHIRPS, the event is made 4.4 times more likely and ~15% wetter due to 1.3C warming of the world due to human-induced climate change.

Urán-Zea (2015) analyzed changes in extreme precipitation using in-situ data over the Aburra Valley in Colombia, where the landslides in Granizal occurred, finding positive trends in extreme precipitation (percentiles 66 to 99) at subdaily time-scales (less than 12 hours), evidencing increases in short duration heavy precipitation over the region, at least for the period 1996-2015. However, due to the rapid timeframe of our analysis, there was not enough time to acquire and apply long-term weather station data to evaluate the gridded datasets. Therefore, we do not discard any of these gridded datasets. We note that, given the complex topographic patterns and climatic drivers, future studies should prioritise validating gridded products using high-quality weather station data to enable a more robust and insightful interpretation of the observed trends.

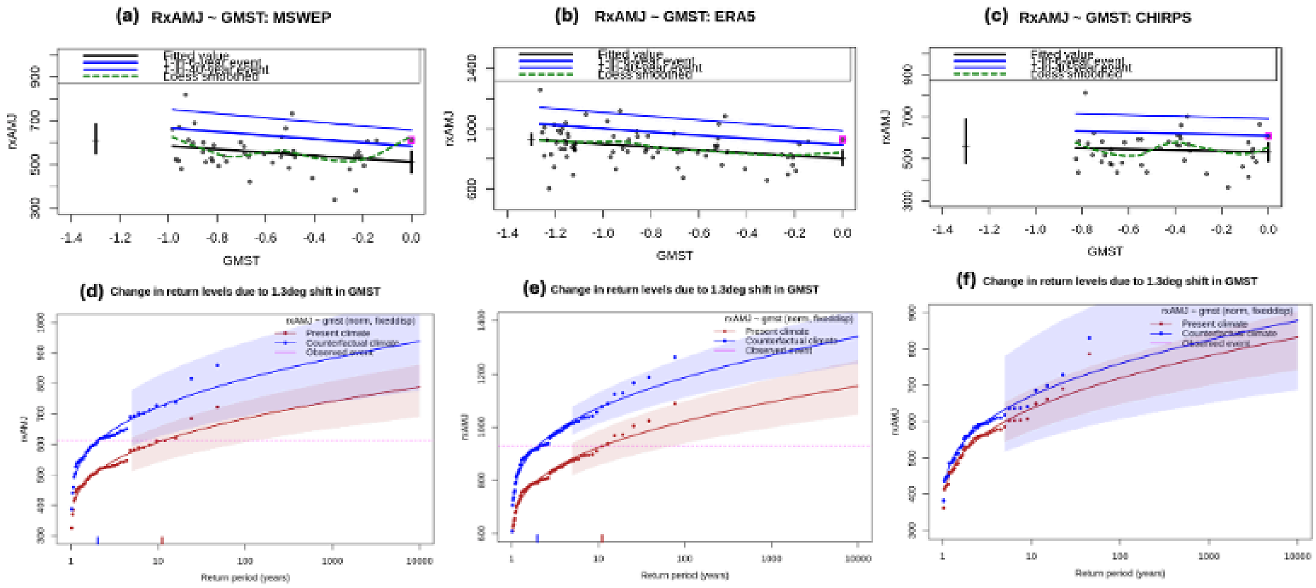

Figure 3.1 *Gaussian fit with fixed dispersion parameter scaling proportional to GMST of the index series.* ***(a-c)*** *Observed AMJ cumulative rainfall [mm] as a function of the smoothed GMST. The thick black line denotes the time-varying location parameter. The vertical black lines show the 95% confidence interval for the location parameter, for the current, 2025 climate and the fictional, 1.3ºC cooler climate. The 2025 observation is highlighted with the magenta box.* ***(d-f)*** *Return time plots for the climate of 2025 (red) and a climate with GMST 1.3 ºC cooler (blue). The past observations are shown twice: once shifted up to the current climate and once shifted down to the climate of the pre-industrial era. The markers show the data and the lines show the fits and uncertainty from the bootstrap. The magenta line shows the magnitude of the 2025 event analysed here. These are shown for MSWEP (left panels), ERA5 (middle panels) and CHIRPS (right panels). Note that CHIRPS did not have data covering the event at the time of doing this analysis.*

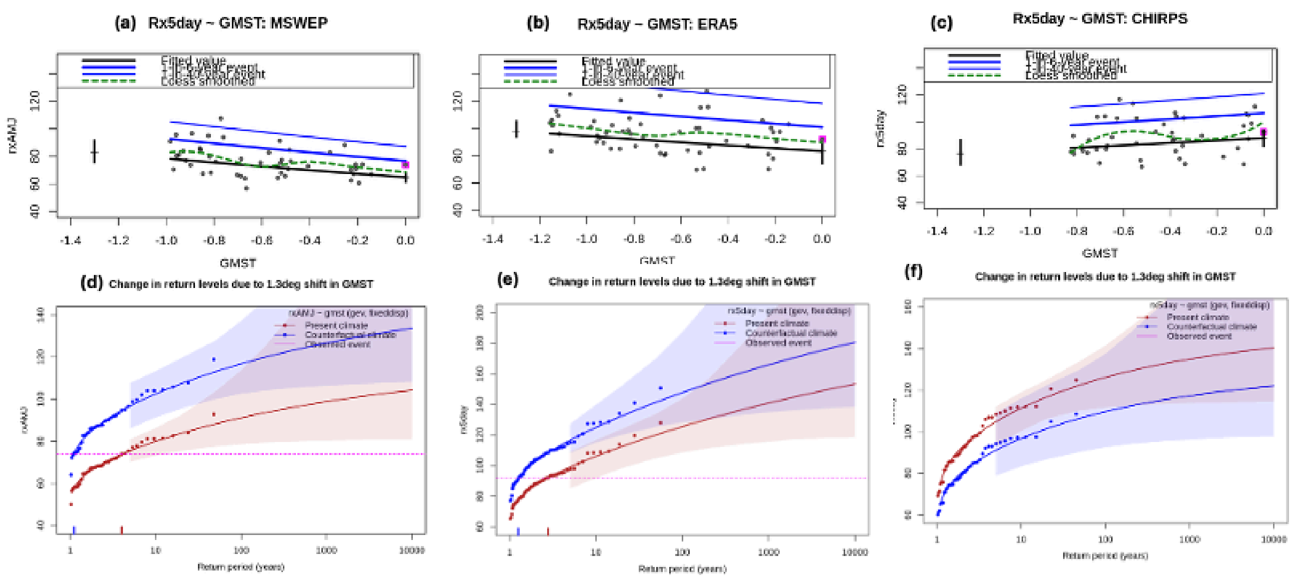

Figure 3.2 *GEV fit with fixed dispersion and location parameter scaling proportional to GMST of the index series.* ***(a-c)*** *Observed annual max.5-day cumulative rainfall [mm/5day] as a function of the smoothed GMST. The thick black line denotes the time-varying location parameter. The vertical black lines show the 95% confidence interval for the location parameter, for the current, 2025 climate and the fictional, 1.3ºC cooler climate. The 2025 observation is highlighted with the magenta box.* ***(d-f)*** *Return time plots for the climate of 2025 (red) and a climate with GMST 1.3 ºC cooler (blue). The past observations are shown twice: once shifted up to the current climate and once shifted down to the climate of the pre-industrial era. The markers show the data and the lines show the fits and uncertainty from the bootstrap. The magenta line shows the magnitude of the 2025 event analysed here. These are shown for MSWEP (left panels), ERA5 (middle panels) and CHIRPS (right panels). Note that CHIRPS did not have data covering the event at the time of doing this analysis.*

Table 3.1. Estimated return periods of AMJ rain and annual Rx5day events over the Colombian Andes and Venezuelan Llanos regions, respectively, in the three selected datasets. Note that the event is not covered in CHIRPS at the time of doing this study. Therefore, the event magnitudes are estimated for return periods of 10 years and 3 years, respectively, that are arrived at from the other two datasets that have coverage of the event.

Dataset	AMJ rain		Annual Rx5day	
	Magnitude (mm)	Return period (95% C.I.)	Magnitude (mm/5day)	Return period (95% C.I.)
MSWEP	611.4484	11 (4.1 ... 1.2e+2)	73.8361053	4.0 (2.3 ... 12)
ERA5	928.03937	11 (4.3 ... 68)	92.05958557	2.8 (1.6 ... 10)
CHIRPS	636.041516	10	98.8055032	3.0

Table 3.2. Change in probability ratio and magnitude for AMJ rain and annual Rx5day events over the Colombian Andes and Venezuelan Llanos regions, respectively, due to GMST.

Dataset	GMST (AMJ rain)		GMST (Annual Rx5day)	
	Probability Ratio	Change in magnitude (%)	Probability Ratio	Change in magnitude (%)
MSWEP	0.18 (0.013 ... 1.5)	-16 (-32 ... 3.4)	0.28 (0.092 ... 0.63)	-22 (-34 ... -7.9)
ERA5	0.18 (0.024 ... 0.56)	-14 (-23 ... -5.1)	0.45 (0.11 ... 0.89)	-15 (-32 ... -2.7)
CHIRPS	0.52 (0.12 ... 5.3e+2)	-5.3 (-29 ... 26)	4.4 (0.52 ... ∞)	15 (-11 ... 38)

4 Model evaluation

In the subsections below, we show the results of the model evaluation for each location. The climate models are evaluated against the observations in their ability to capture:

1. Seasonal cycles: For this, we qualitatively compare the seasonal cycles based on model outputs against observations-based cycles. We discard the models that exhibit ill-defined peaks in their seasonal cycles. We also discard the model if the rainy season onset/termination varies significantly from the observations.

2. Spatial patterns: Models that do not match the observations in terms of the large-scale precipitation patterns are excluded.

3. Parameters of the fitted statistical models: We discard the model if the model and observation parameters ranges do not overlap.

The models are labelled as ‘good’,’reasonable’, or ’bad’ based on their performances in terms of the three criteria discussed above. A model is given an overall rating of ‘good’ if it is rated ‘good’ for all three characteristics. If there is at least one ‘reasonable’, then its overall rating will be ‘reasonable’ and ‘bad’ if there is at least one ‘bad’. For each framing or model setup we also use models that only just pass the evaluation tests if we only have five models or less for that framing that perform well.

4.1 AMJ Rainfall over the Colombian Andes

Tables 4.1 and 4.2 show the results for model evaluation in their performance for AMJ total precipitation in the Colombian Andes and for annual Rx5day in the Venezuelan Llanos, respectively.

Table 4.1 *Evaluation results of the climate models considered for attribution analysis of AMJ cumulative precipitation in the Colombian Andes. For each model, the threshold for a 1-in-10-year event is shown, along with the best estimates of the Dispersion parameters are shown, along with 95% confidence intervals. Furthermore evaluation of the seasonal cycle and spatial pattern are shown.*

Model / Observations	**Seasonal cycle**	**Spatial pattern**	**Dispersion**	**Conclusion**
MSWEP			0.145 (0.105 ... 0.175)	
ERA5			0.119 (0.0951 ... 0.140)	
CHIRPS			0.151 (0.111 ... 0.180)	
HighResMIP ()			(...)	
CMCC-CM2-HR4 ()	bad	reasonable	0.178 (0.147 ... 0.208)	bad

CMCC-CM2-VHR4 ()	bad	reasonable	0.138 (0.115 ... 0.159)	bad
CNRM-CM6-1 ()	good	good	0.111 (0.0935 ... 0.127)	good
CNRM-CM6-1-HR ()	good	good	0.119 (0.0996 ... 0.133)	good
EC-Earth3P ()	good	good	0.126 (0.0928 ... 0.153)	good
EC-Earth3P-HR ()	good	good	0.124 (0.0880 ... 0.155)	good
HadGEM3-GC31-HM ()	good	reasonable	0.0996 (0.0792 ... 0.119)	reasonable
HadGEM3-GC31-LM ()	good	bad	0.104 (0.0880 ... 0.116)	bad
HadGEM3-GC31-MM ()	good	reasonable	0.118 (0.0986 ... 0.134)	reasonable
MPI-ESM1-2-HR ()	bad	bad	0.123 (0.102 ... 0.139)	bad
MPI-ESM1-2-XR ()	good	reasonable	0.117 (0.0956 ... 0.136)	reasonable
cordex ()			(...)	
HadGEM2-ES_GERICS-REMO2015 ()	good	reasonable	0.147 (0.118 ... 0.173)	reasonable
HadGEM2-ES_ICTP-RegCM4-7 ()	bad	reasonable	0.172 (0.139 ... 0.202)	bad
MPI-ESM-LR_GERICS-REMO2015 ()	reasonable	reasonable	0.135 (0.110 ... 0.153)	reasonable
MPI-ESM-MR_ICTP-RegCM4-7 ()	bad	reasonable	0.258 (0.198 ... 0.287)	bad
NorESM1-M_GERICS-REMO2015 ()	reasonable	reasonable	0.169 (0.138 ... 0.191)	reasonable
NorESM1-M_ICTP-RegCM4-7 ()	bad	reasonable	0.237 (0.192 ... 0.279)	bad

4.2 Annual 5-day maximum rainfall over the Venezuelan Llanos

Table 4.2 *Evaluation results of the climate models considered for attribution analysis of annual Rx5day over the Venezuelan Llanos. For each model, the threshold for a 1-in-3-year event is shown, along with the best estimates of the Dispersion and Shape parameters are shown, along with 95% confidence intervals. Furthermore evaluation of the seasonal cycle and spatial pattern are shown.*

Model / Observations	**Seasonal cycle**	**Spatial pattern**	**Dispersion**	**Shape parameter**	**Conclusion**
MSWEP			0.122 (0.0864 ... 0.146)	-0.15 (-0.49 ... 0.19)	
ERA5			0.134 (0.100 ... 0.156)	-0.090 (-0.30 ... 0.18)	

CHIRPS			0.147 (0.112 ... 0.176)	-0.21 (-0.56 ... 0.090)	
HighResMIP ()			(...)	(...)	
CMCC-CM2-HR4 ()	bad	reasonable	0.132 (0.105 ... 0.153)	-0.22 (-0.42 ... -0.096)	bad
CMCC-CM2-VHR4 ()	reasonable	reasonable	0.106 (0.0805 ... 0.123)	-0.28 (-0.48 ... -0.10)	reasonable
CNRM-CM6-1 ()	good	good	0.0913 (0.0752 ... 0.103)	-0.17 (-0.36 ... 0.0048)	good
CNRM-CM6-1-HR ()	reasonable	good	0.0661 (0.0531 ... 0.0751)	-0.21 (-0.43 ... -0.063)	bad
EC-Earth3P ()	good	good	0.0435 (0.0329 ... 0.0501)	-0.068 (-0.35 ... 0.10)	bad
EC-Earth3P-HR ()	good	good	0.0498 (0.0395 ... 0.0572)	-0.12 (-0.41 ... 0.064)	bad
HadGEM3-GC31-HM ()	reasonable	reasonable	0.0711 (0.0580 ... 0.0821)	-0.13 (-0.35 ... 0.048)	bad
HadGEM3-GC31-LM ()	good	bad	0.105 (0.0844 ... 0.123)	-0.17 (-0.35 ... 0.031)	bad
HadGEM3-GC31-MM ()	reasonable	reasonable	0.0993 (0.0804 ... 0.114)	-0.27 (-0.47 ... -0.12)	reasonable
MPI-ESM1-2-HR ()	bad	bad	0.0728 (0.0568 ... 0.0861)	-0.24 (-0.40 ... -0.066)	bad
MPI-ESM1-2-XR ()	bad	reasonable	0.0547 (0.0448 ... 0.0626)	-0.11 (-0.28 ... 0.011)	bad
cordex ()			(...)	(...)	
HadGEM2-ES_GERICS-REMO2015 ()	bad	reasonable	0.120 (0.0952 ... 0.143)	-0.14 (-0.45 ... 0.060)	bad
HadGEM2-ES_ICTP-RegCM4-7 ()	reasonable	reasonable	0.180 (0.133 ... 0.214)	-0.17 (-0.50 ... 0.034)	reasonable
MPI-ESM-LR_GERICS-REMO2015 ()	bad	reasonable	0.0884 (0.0689 ... 0.102)	-0.30 (-0.65 ... -0.15)	bad
MPI-ESM-MR_ICTP-RegCM4-7 ()	reasonable	reasonable	0.165 (0.129 ... 0.190)	-0.11 (-0.39 ... 0.096)	reasonable
NorESM1-M_GERICS-REMO2015 ()	reasonable	reasonable	0.0906 (0.0738 ... 0.104)	-0.043 (-0.32 ... 0.15)	reasonable
NorESM1-M_ICTP-RegCM4-7 ()	reasonable	reasonable	0.213 (0.154 ... 0.252)	-0.21 (-0.41 ... -0.032)	reasonable

5 Multi-method multi-model attribution

This section shows Probability Ratios (PR) and change in intensity (ΔI) for models that passed model evaluation and also includes the values calculated from the fits with observations. Tables 5.1 and 5.2 summarise the results.

5.1 AMJ Rainfall over the Colombian Andes

Table 5.1. *Event magnitude, probability ratio and change in intensity for 10-year return period for AMJ rainfall in the Colombian Andes for observational datasets and each model that passed the evaluation tests. (a) from pre-industrial climate to the present and (b) from the present to 2.6℃ above pre-industrial climate.*

		a. Past vs. present		b. Present vs. future	
Model / Observations	**Threshold for return period 10 yr**	**Probability ratio PR [-]**	**Change in intensity ΔI [units]**	**Probability ratio PR [-]**	**Change in intensity ΔI [units]**
MSWEP	611.4484 mm	0.18 (0.013 ... 1.5)	-16 (-32 ... 3.4)		
ERA5	928.03937 mm	0.18 (0.024 ... 0.56)	-14 (-23 ... -5.1)		
CHIRPS	636.041516 mm	0.52 (0.12 ... 5.3e+2)	-5.3 (-29 ... 26)		
CNRM-CM6-1 ()	1.0e+3 mm	0.58 (0.21 ... 3.2)	-3.3 (-11 ... 5.2)	(...)	(...)
CNRM-CM6-1-HR ()	7.9e+2 mm	0.54 (0.19 ... 2.5)	-4.0 (-13 ... 4.6)	(...)	(...)
EC-Earth3P ()	9.4e+2 mm	3.3 (0.36 ... 1.2e+2)	6.5 (-6.4 ... 21)	(...)	(...)
EC-Earth3P-HR ()	9.8e+2 mm	11 (0.73 ... 8.8e+2)	12 (-1.5 ... 30)	(...)	(...)
HadGEM3-GC31-HM ()	1.1e+3 mm	1.6 (0.45 ... 13)	2.2 (-4.5 ... 9.5)	(...)	(...)
HadGEM3-GC31-MM ()	1.0e+3 mm	1.5 (0.33 ... 18)	2.3 (-7.3 ... 13)	(...)	(...)
MPI-ESM1-2-XR ()	9.3e+2 mm	0.45 (0.17 ... 2.5)	-5.3 (-15 ... 4.8)	(...)	(...)
HadGEM2-ES_GERICS-REMO2015 ()	7.7e+2 mm	0.36 (0.18 ... 1.0)	-8.6 (-16 ... 0.034)	0.95 (0.60 ... 1.4)	-0.38 (-3.6 ... 2.6)
MPI-ESM-LR_GERICS-REMO2015 ()	6.3e+2 mm	0.14 (0.11 ... 0.27)	-21 (-29 ... -11)	0.38 (0.17 ... 0.71)	-6.0 (-9.8 ... -2.3)
NorESM1-M_GERICS-REMO2015 ()	3.9e+2 mm	0.32 (0.15 ... 2.5)	-11 (-24 ... 6.0)	0.27 (0.088 ... 0.61)	-9.2 (-15 ... -3.7)

5.2 Annual 5-day maximum rainfall over the Venezuelan Llanos

Table 5.2. *Event magnitude, probability ratio and change in intensity for 3-year return period for annual Rx5day in the Venezuelan Llanos for observational datasets and each model that passed the evaluation tests. (a) from pre-industrial climate to the present and (b) from the present to 2.6℃ above pre-industrial climate.*

		a. Past vs. present		b. Present vs. future	
Model / Observations	**Threshold for return period 3 yr**	**Probability ratio PR [-]**	**Change in intensity ΔI [%]**	**Probability ratio PR [-]**	**Change in intensity ΔI [%]**
MSWEP	73.8361053 mm/5day	0.28 (0.092 ... 0.63)	-22 (-34 ... -7.9)		
ERA5	92.05958557 mm/5day	0.45 (0.11 ... 0.89)	-15 (-32 ... -2.7)		
CHIRPS	98.8055032 mm/5day	4.4 (0.52 ... 2.8e+3)	15 (-11 ... 38)		
CMCC-CM2-VHR4 ()	2.1e+2 mm/5day	3.0 (0.93 ... ∞)	8.0 (-0.77 ... 18)	(...)	(...)
CNRM-CM6-1 ()	1.2e+2 mm/5day	0.98 (0.50 ... 4.9)	-0.18 (-7.4 ... 9.4)	(...)	(...)
HadGEM3-GC31-MM ()	1.8e+2 mm/5day	1.5 (0.63 ... 23)	3.1 (-4.7 ... 12)	(...)	(...)
HadGEM2-ES_ICTP-RegCM4-7 ()	1.9e+2 mm/5day	1.1 (0.53 ... 2.9)	1.6 (-12 ... 14)	0.98 (0.77 ... 1.2)	-0.28 (-4.1 ... 3.4)
MPI-ESM-MR_ICTP-RegCM4-7 ()	1.7e+2 mm/5day	0.34 (0.33 ... 0.39)	-33 (-42 ... -22)	0.56 (0.26 ... 0.85)	-9.8 (-16 ... -3.2)
NorESM1-M_GERICS-REMO2015 ()	1.5e+2 mm/5day	0.64 (0.36 ... 4.3)	-4.8 (-14 ... 11)	0.88 (0.62 ... 1.2)	-1.3 (-4.3 ... 1.8)
NorESM1-M_ICTP-RegCM4-7 ()	1.2e+2 mm/5day	0.34 (0.33 ... 0.37)	-44 (-54 ... -33)	0.29 (0.064 ... 0.47)	-22 (-29 ... -15)

6 Hazard synthesis

For the event definitions described in Section 1.2, we evaluate the influence of anthropogenic climate change on the events by calculating the probability ratio as well as the change in intensity using observations and climate models. Models which do not pass the evaluation described above are excluded from the analysis. The aim is to synthesise results from models that pass the evaluation along with the observations-based products to give an overarching attribution statement.

Figures 6.1-6.2 show the changes in probability and intensity for the observations (blue) and models (red). Before combining them into a synthesised assessment, first, a representation error is added (in quadrature) to the observations, to account for the difference between observations-based datasets that cannot be explained by natural variability. This is shown in Figures 6.1-6.2 as white boxes around the light blue bars. The dark blue bar shows the average over the observation-based products. Next, a term to account for inter-model spread is added (in quadrature) to the natural variability of the models. This is shown in Figures 6.1-6.2 as white boxes around the light red bars. The dark red bar shows the model average, consisting of a weighted mean using the (uncorrelated) uncertainties due to natural variability plus the term representing inter-model spread (i.e., the inverse square of the white bars).

Observation-based products and models are combined into a single result in two ways. Firstly, we neglect common model uncertainties beyond the inter-model spread that is depicted by the model average, and compute the weighted average of models (dark red bar) and observations (dark blue bar): this is indicated by the magenta bar. As model uncertainty can be larger than inter-model spread due to common model uncertainties, secondly, we also show the more conservative estimate of an unweighted, direct average of observations (dark blue bar) and models (dark red bar) contributing 50% each, indicated by the white box around the magenta bar in the synthesis figures. Due to the fact that models as well as observation-based products show very different results, the weighted and unweighted synthesis is almost identical, representing large uncertainties that show no very clear signal for both event definitions.

While the average of the observations shows a drying trend, with a 12% decrease in the AMJ rainfall in the Colombian Andes region and a 9% decrease in annual Rx5day in the Venezuelan Llanos region, the trend in seasonal rainfall is less pronounced in the CHIRPS dataset for the Colombian Andes region. The same dataset shows an increasing trend in the case of Rx5day over the Llanos region, albeit with large uncertainties. However, due to difficulties in accessing long-term quality-controlled weather observations within the timeframe of this rapid study, we cannot conclusively rule out one or more of the datasets. As a consequence, we do not have much confidence in the quantitative estimates.

In both cases, the climate models show quantitatively similar results to the observation-based products, again with opposing signs in some models. The synthesised results give an overall decrease of about 6% for the AMJ Colombian Andes region and about 8% for Rx5day in the Venezuelan Llanos, both with very large uncertainties (see Table 6.1) that are more centred around zero for the Rx5day event. Based on these results as well as the published literature (see Section 1.1) that also shows very large uncertainties, we cannot give a confident assessment of the role of climate change. For the future, existing literature consistently projects a drying of seasonal rainfall over the NSA region which contains the studied region in the Colombian Andes, especially during June, July, and August, alongside an increased likelihood and intensity of heavy rainfall events (low confidence), such as Rx5day, which begins to emerge only under higher future warming of 3°C above pre-industrial levels. In this study, we see a similar result, with a drying projected for the AMJ event and a less strong and not-significant drying for the Rx5day event. As only three of the models that passed the evaluation did have future simulations, these are again not confident results.

Overall, we conclude that while wet years like the recent ones will continue to occur, the more consistent drying observed in the eastern parts of the region points to a rising risk of dry years. This highlights the need for preparedness against both more frequent and intense droughts and wildfires, as well as the potential for extreme downpours. Notably, even regions undergoing long-term drying trends may see increases in short, intense rainfall bursts, adding further complexity to future climate risks (e.g., Bauer et al., 2024; Laz et al., 2014).

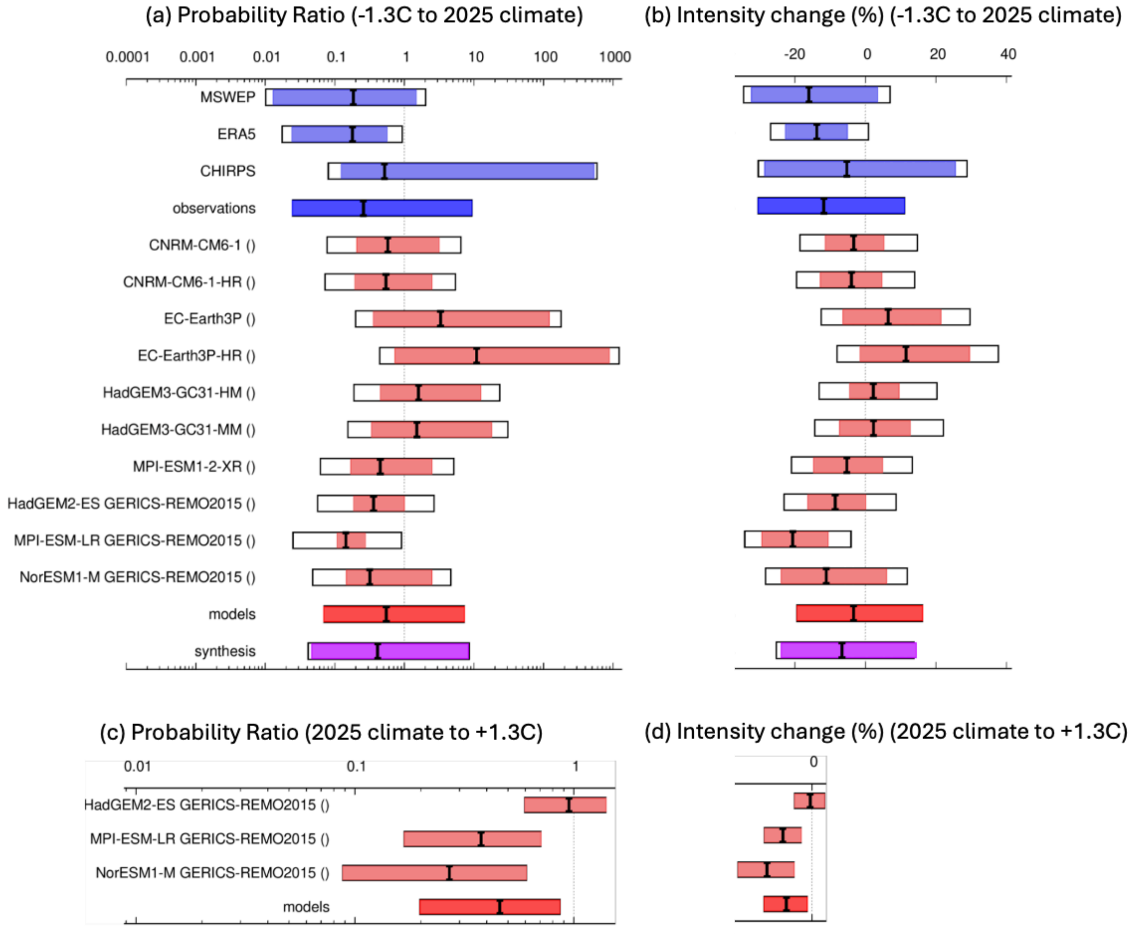

***Figure 6.1**: Synthesis of (a) probability ratios and (b) intensity change when comparing AMJ rainfall over the study region over the Colombian Andes with a 1.3℃ cooler climate. (c) same as (a) and (d) same as (b) when comparing the event with a 1.3℃ warmer climate.*

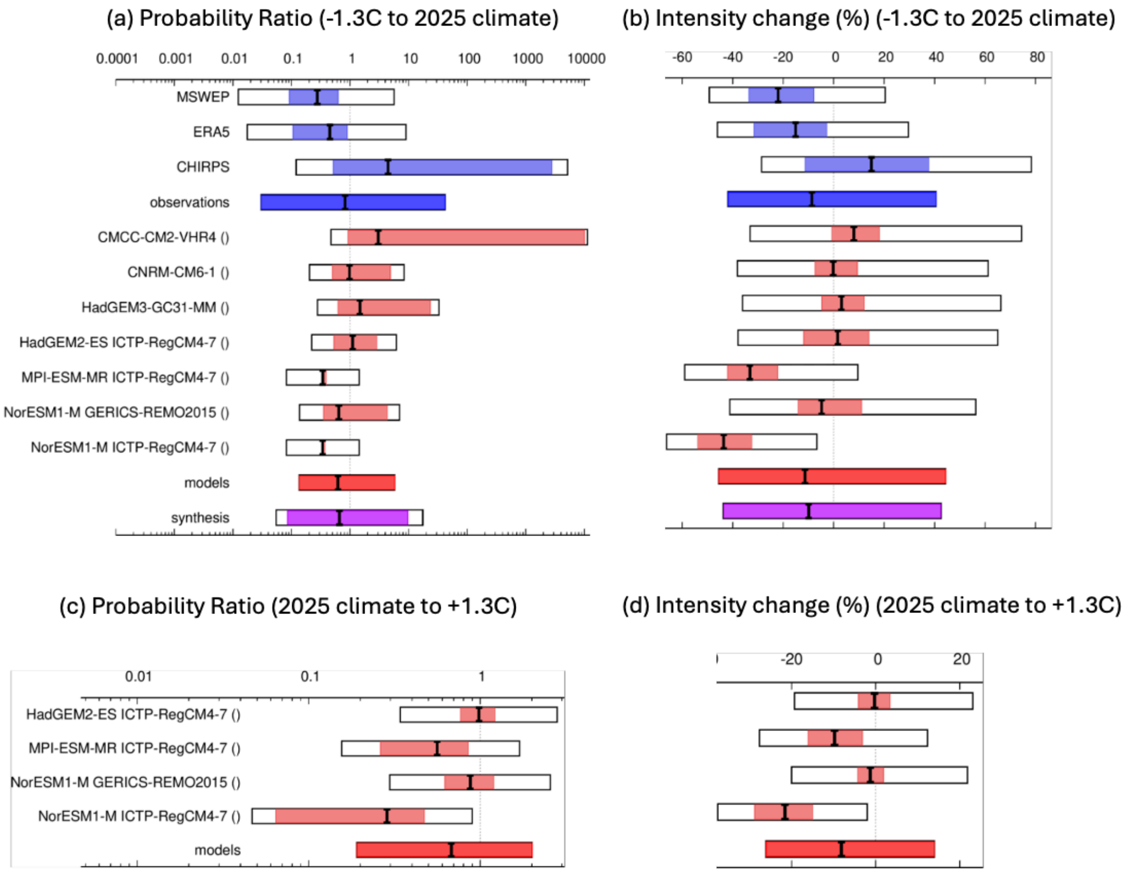

Figure 6.2: *Synthesis of (a) probability ratios and (b) intensity change when comparing annual Rx5day over the study region over the Venezuelan Llanos with a 1.3℃ cooler climate. (c) same as (a) and (d) same as (b) when comparing the event with a 1.3℃ warmer climate.*

Table 6.1: *Summary of results for (a) 1-in-10 year AMJ rain in the Colombian Andes and (b) 1-in-3 year annual Rx5day in the Venezuelan Llanos, presented in Figs (6.1-6.2): changes due to GMST include past-present changes and present-future changes.*

Data		**AMJ rain**		**Rx5day**	
		Probability ratio (95% CI)	**Intensity change (%) (95% CI)**	**Probability ratio (95% CI)**	**Intensity change (%) (95% CI)**
Observations	**Past-Present**	0.257 (0.0245 … 9.33	-11.8 (-30.4 … 11.1)	0.823 (0.0303 … 41.9)	-8.66 (-41.9 … 40.6)
Models		0.549 (0.0697 … 7.27)	-3.34 (-19.4 … 16.2)	0.621 (0.135 … 5.81)	-11.4 (-45.5 … 44.4)
Synthesis		0.412 (0.0467 … 8.32)	-6.64 (-23.9 … 14.4)	0.659 (0.0857 … 9.69)	-9.89 (-43.6 … 42.4)
Models only	**Present-Future**	0.459 (0.198 … 0.863)	-5.28 (-9.85 … -0.991)	0.678 (0.191 … 2.01)	-8.15 (-26.1 … 13.9)

7 Vulnerability and exposure

Following more than four consecutive days of intense rainfall, reports indicate significant damage caused by landslides, strong winds, and river flooding in Colombia and Venezuela. The volume and speed of the water damaged infrastructure, washing away bridges, blocking roads, and isolating numerous indigenous, Afro-descendant, and farmer communities (Mazo González, 2025). In Colombia the city of Medellin and Bello have been particularly hard hit, while in Venezuela the western and northern parts of the country, especially Merida, Trujillo and Tachira states have been affected by floods and landslides (ERCC, 2025). According to satellite imagery of the floods, over 2 million Ha were flooded in Venezuela, with nearly 900,000 hectares (Ha) of that area being agricultural cropland (USDA, 2025). The impacts of the extreme rainfall, floods and landslides are spread out geographically, but the vulnerability and exposure to the particular hazard is very local. Given the rapid nature of this study, this section focuses on vulnerability and exposure in Colombia, especially to landslides given the significant impacts during this event.

Overall, approximately 85% of the Colombian population lives in areas exposed to two or more natural hazards, including floods, droughts and cyclones. Floods have historically been the most frequent natural hazard (70%), with the greatest impact on populations (World Bank, 2025). The Magdalena River is Colombia's principal waterway, supporting nearly 80% of the country's population and a significant portion of its economy (Escobar & Wickel, 2015) According to the National Unit for Disaster Risk Management (UNGRD) in Colombia, at least 2,065,725 people were affected or displaced due to wildfires, landslides, floods, strong winds, and water shortages in 2024, representing a 417% increase compared to 2023 (OCHA, 2024). The Antioquia region has experienced numerous flood and landslide events in recent years, including January 2023 when flash floods led to at least two deaths and 23 injured in Medellín, March-April 2022 floods and landslides across the state affecting hundreds of people and killing at least 12, and May 2015 in the town of Salgar when over 100 people died and 535 houses were destroyed (ECHO, 2023; Hoyos et al., 2019; Floodlist, 2022). These events posed serious threats to food security, public health, and livelihoods (OCHA, 2024). In response to the prolonged and intense rainfall that year, the government declared a nationwide state of emergency, lasting twelve months, to expedite aid and recovery efforts. This sequence of disasters laid the groundwork for the compounded impacts witnessed in the current year's flooding, further straining already weakened systems and communities.

Historically, one of the most devastating debris flows in Colombia occurred in 2017 over the Andes-Amazon transition region. This event occurred during the early morning of April 1st, 2017, in the city of Mocoa, Putumayo. There was a heavy precipitation event between March 31st 19:00 Local Time (LT) and April 1st 03:00 LT, with higher activity about March 31st 22:00 LT. The 24-hour accumulated precipitation during this event corresponds to the fourth largest on record during the period 1984-2022 (Martínez et al., 2024), which, in conjunction with the precipitation accumulated during the previous 4 days, produced the overflow of the Mocoa, Mulato and Sangoyaco rivers (Prada-Sarmiento et al., 2020). As a consequence, more than 600 shallow landslides were triggered, causing a huge debris flow with significant impacts (Cheng et al., 2018; García-Delgado et al., 2019; Prada-Sarmiento et al., 2020). This debris flow caused most of the casualties (about 300 human lives) and damages and was not considered in the pre-event local hazard map (Prada-Sarmiento et al., 2020).

This analysis will examine non-climatic drivers of flood risk, including land use land cover changes, urban planning practices, informality, governance dynamics, adaptation, early warning systems, and disaster response mechanisms.

7.1 Land-use Changes, Urban Planning, and Informality

Landslides are common in Colombia, where steep slopes, high population density and seasonal rainfall contribute to their occurrence and high death toll (Sepúlveda and Petley, 2015). A majority (>90%) of landslides registered in national databases were triggered by rainfall (Aristizábal & Sánchez, 2019). Medellin is a fast growing city that is particularly vulnerable to landslides due to the combination of steep slopes, landslide-prone dunite rock, and high exposure of populations many of whom live in informal settlements (Gamper et al., 2023). Between 1994 and 2018, a satellite analysis showed that urban areas in Medellin exposed to landslide risks (medium and high hazard levels) have tripled (Kuhnl, 2022). The analysis also found that informal settlements are more exposed to landslide hazards than formal ones, but that more formal settlements are also being established on exposed slopes than before (Ibid).

Urbanization in Colombia is linked to a variety of factors including population growth, industrialisation in cities, people moving from rural to urban areas due to economic reasons and internal displacement due to conflict or violence (Sanchez, 2007; Guzman et al., 2018). The growth of informal settlements in Colombia in turn is linked to factors like the rate and unplanned nature of urbanization, and a lack of available land (Kuhnl, 2022). In Colombia, between the 1970s and early 2010s, more than half of the houses destroyed by floods, landslides, volcanic eruptions, earthquakes, and other disasters have been built in areas considered unsuitable for urban development, with floods accounting for the majority of this destruction (GFDRR, 2014). Granizal village near where the landslide occurred is known to be an area with a high degree of informality, and many of the people are internally displaced (OpenHandsInitiative, 2025).

In addition to urban areas, the Páramos are the high-mountain wetlands located atop the Andes which play an important role in capturing water during the rainy season and acting as natural barriers against floods (Murad et al. 2024; Scientific American, 2012). Factors like the conversion to agricultural land, overgrazing, mining concessions and building of roads are contributing to the degradation of the Paramos, reducing the vital natural protection that it provides (Murad et al. 2024.). A similar situation applies to the *humedales*, wetlands found in moorlands, swamps, and mangroves, which function as natural water regulators in the vast and agriculturally productive savannas downstream.

Since the 1970s, the Andean and lowland regions of the Magdalena basin have undergone extensive deforestation. Over a 20-year period, pasture and agricultural land increased by 65% while forest cover decreased by 40% (Restrepo & Syvitski, 2006). By 2000, nearly 69% of Andean forests and 30% of lowland forests were lost (Salgado et al., 2022). This has been driven by the expansion of agriculture, including industrial crops such as palm oil, pasture, and urbanization. A study of landslides in the Colombia Andes found that landslides are approximately six times more likely to occur on non-forested lands than forested ones and it is 16 times more cost-effective to pay for forest conservation or restoration than to pay the expected value of landslide damage (Grima et al., 2020). Adaptation efforts like forest corridors, reforestation, payment for ecosystem services can therefore be extremely valuable and effective.

7.2 Flood risk management

7.2.1 Adaptation

In the Magdalena River basin in Colombia, polder systems, reclaimed low-lying lands protected by dikes and managed through irrigation and drainage infrastructure, constitute a key pillar of its flood protection system. The RUT Irrigation District features a 44 km dike along the river, a flood interceptor canal, and pumping stations to manage both drainage and irrigation. Water is pumped out during wet seasons and in for irrigation during dry periods (Shultz, 2025). Canal del Dique and the Polders of Mompós use similar flood protection and water management systems (Ibid). A major distributary of the Magdalena River, Canal del Dique suffered severe flooding in 2010, after which a comprehensive restoration and flood protection project was launched. Measures include regulating the inlet of water from the river, with a control structure managed by an automated system using SCADA and Delft-FEWS, a flood forecasting software (Sokolewicz et al., 2016). The Mompos Depression, one of the world's biggest wetland systems, is routinely inundated by Magdalena River floods. Hydropower by Design is a basin-wide integrated floodplain management and planning approach which uses modeling tools such as WEAP to assess impacts of upstream water resource developments on flood patterns and characteristics (Escobar & Wickel, 2015). Further, projects implemented over recent years have developed Decision Support Systems (DSS) tools to help water users across the basin to monitor water demand, availability, and quality, which supports adaptive management and targeted interventions for both flood protection and drought mitigation (Bazin et al., 2022). Other recent measures in the river basin focus on ecosystem-based adaptation. For example, The Nature Conservancy (TNC), the International Union for Conservation of NAture (IUCN), and Colombian authorities have led projects to restore wetlands and floodplains, sustainable land use, and integrating ecosystem services into public planning, promoting natural flood regulation to reduce vulnerability to flooding and maintain vital ecosystem services for millions living in the basin (Lamus, Grueso & Casas, 2019; Murillo et al., 2018; Virida Projects, 2024).

7.2.2 Early Warning Systems and Response

Colombia has made significant progress in establishing flood early warning systems across levels of government, integrating advanced technology, institutional coordination, and community engagement. One example is the Piragua program, operated by CORANTIOQUIA, one of the environmental authorities in the country. This system operates in 80 municipalities of the region, combining community-based measurements using low-cost instruments and technology-based measurements from meteorological/limnographic stations (Arias et al., 2016). Also, the Sistema de Alerta Temprana de Medellín y el Valle de Aburrá (SIATA), a model multi-hazard early warning system, provides real-time alerts for floods, landslides, wildfires, and other hazards to over 2.5 million residents in the Medellín and Aburrá Valley (Palmer, 2023). Following the landslide in Granizal, SIATA were deployed to install alert sirens in case of further landslides (The Watchers, 2025). Further, in Medellín, a low-cost, community-based landslide early warning system has been piloted in an informal hillside settlement. A study by Gamperl et al. (2023) demonstrates its technical viability, while highlighting the critical role of sustained community involvement and institutional support for long-term effectiveness. Colombia's National Unit for Disaster Risk Management (UNGRD), in partnership with the Pacific Disaster Center, has also completed a comprehensive risk and vulnerability assessment for all 1,122 municipalities, enabling tailored early warning protocols and targeted investments at local levels (PDC, 2025). In flood-prone wetland regions, such as La Mojana, communities have developed their own early warning systems in partnership with local governments and the Institute of Hydrology, Meteorology, and Environmental Studies (IDEAM) (Jimenez, 2025). Community residents monitor river levels, identify risk zones, and coordinate evacuation and contingency plans. Further, the Colombian Red Cross is scaling community early warning systems and anticipatory action protocols for both floods and droughts. This includes forming local emergency response teams and updating contingency plans, empowering communities to anticipate and respond to extreme weather events (Cruz Roja Colombiana & IFRC, 2025).

In response, local authorities have appealed for national assistance and emergency support, including the deployment of medical brigades, the distribution of emergency kits, and the provision of machinery to clear roads and improve access to the most severely affected areas (Caracol, 2025).

7.3 Governance

The political and historical conflict dynamics in Colombia intensify the impacts of floods and storms by increasing the vulnerability of populations, limiting available support, and making institutional responses challenging especially in the most isolated areas where the road network and general infrastructure are limited (ICRC, 2025). The spatial overlap between areas affected by the 60 years of armed conflict and regions highly exposed to climate hazards creates scenarios of dual vulnerability. Numerous studies have documented that many of the areas impacted by floods also coincide with regions historically marked by violence and forced displacement, which makes the planning and implementation of disaster risk reduction strategies more difficult (IECAH, 2011).

The institutional weakness in parts of the national territory, especially those affected by the conflict and the state fragmentation in areas with the presence of non-state armed groups (NSAG) limits the coverage of public services and obstruct the execution of risk management policies. Limited technical and financial capacity in areas affected by poverty and the legacy of conflict at the municipal level increases community exposure, while territorial control by armed groups discourages both public and private investment in resilient infrastructure (GFDRR, 2012).

Additionally, the persistence or escalation of conflict in regions such as Catatumbo, Arauca, o and Chocó generates new mass displacements and severely restricts humanitarian access during climate emergencies. In 2025, clashes between armed groups in these areas left tens of thousands of people without essential assistance (MSF, 2025). This is further compounded by cuts to international funding, such as the downsizing of the UN Human Rights Office's operations in Colombia and other UN agencies, which diminish response capacity in contexts of combined conflict and climate crises (Reuters, 2025).

7.4 V&E Conclusions

Risks associated with extreme rainfall across the Magdalena River basin in Colombia are driven by an interplay of high exposure, environmental degradation, and socio-economic vulnerability. Heavy rainfall in Colombia is relatively common during the rainy season. This combined with landslide prone soil, steep slopes, and river catchments where populations have increasingly settled has largely driven the impacts from flooding and landslides. Additional factors like land-use changes over time (e.g. conversion of the Páramos to agricultural land, overgrazing, and mining concessions) have reduced the natural ecosystems ability to regulate rainfall-induced floods and increased susceptibility to landslides. People who are internally displaced, or affected by conflict are doubly vulnerable. This increased vulnerability combined with recurring climate hazards erodes their resilience over time. Investments in reforestation and forest conservation, and improved water management in informal areas can reduce risks and contribute to adaptation. Colombia has made considerable strides in flood risk management through engineered infrastructure, ecosystem-based adaptation, and advanced early warning systems across governance levels; more work needs to be done to ensure everyone who is at risk is covered by these systems.

Data availability

All time series used in the attribution analysis are available via the Climate Explorer.

References

All references are given as hyperlinks in the text.